

UNCLASSIFIED REPORT DOCUMENTATION PAGEForm Approved
OMB No. 0704-0188

1a. RESTRICTIVE CLASSIFICATION UNCLASSIFIED	1b. RESTRICTIVE MARKINGS
2a. SECURITY CLASSIFICATION AUTHORITY N/A	3. DISTRIBUTION / AVAILABILITY OF REPORT Approved for public release: distribution unlimited
2b. DECLASSIFICATION / DOWNGRADING SCHEDULE N/A	5. MONITORING ORGANIZATION REPORT NUMBER(S) AFOSR-TR. 89-0433
4. PERFORMING ORGANIZATION REPORT NUMBER(S) 3 1989	

DTIC
SELECTED

6a. NAME OF PERFORMING ORGANIZATION Claremont Graduate School	6b. OFFICE SYMBOL (if applicable) D	7a. NAME OF MONITORING ORGANIZATION AFOSR / NM
6c. ADDRESS (City, State, and ZIP Code) Department of Mathematics Claremont, CA 91711	7b. ADDRESS (City, State, and ZIP Code) AFOSR/NM Bolling AFB DC 20332-6448	
8a. NAME OF FUNDING / SPONSORING ORGANIZATION AFOSR/NM	8b. OFFICE SYMBOL (if applicable) NM	9. PROCUREMENT INSTRUMENT IDENTIFICATION NUMBER AFOSR-87-0222
8c. ADDRESS (City, State, and ZIP Code) Building 410, Bolling AFB, DC 20332	10. SOURCE OF FUNDING NUMBERS	
	PROGRAM ELEMENT NO. 61102F	PROJECT NO. 2304
	TASK NO. A 9	WORK UNIT ACCESSION NO.

11. TITLE (Include Security Classification)
THREE-DIMENSIONAL MODELLING FOR CONTACT RESISTANCE OF CURRENT FLOW INTO A SOURCE/DRAIN REGION

12. PERSONAL AUTHOR(S)
DR Ellis Cumberbatch

13a. TYPE OF REPORT Final	13b. TIME COVERED FROM 01 Jun 87 to 31 May 88	14. DATE OF REPORT (Year, Month, Day)	15. PAGE COUNT
------------------------------	--	---------------------------------------	----------------

16. SUPPLEMENTARY NOTATION

17. COSATI CODES	18. SUBJECT TERMS (Continue on reverse if necessary and identify by block number)
FIELD GROUP SUB-GROUP	

19. ABSTRACT (Continue on reverse if necessary and identify by block number)

Various extensions of the transmission line model are introduced to find the resistance for current flow in MOSFET source/drain regions. The geometry is taken to be a rectangular box with a rectangular contact on the upper surface. Explicit formula are derived by assuming that the current flow is restricted to various geometrical planes. Comparison of basic results with simulation and experimental data is good. Comparison with simulation results for misalignment is less good.

20. DISTRIBUTION / AVAILABILITY OF ABSTRACT <input type="checkbox"/> UNCLASSIFIED/UNLIMITED <input type="checkbox"/> SAME AS RPT. <input type="checkbox"/> DTIC USERS	21. ABSTRACT SECURITY CLASSIFICATION UNCLASSIFIED
22a. NAME OF RESPONSIBLE INDIVIDUAL Dr. Arie Nachman	22b. TELEPHONE (Include Area Code) 202-767-4939
	22c. OFFICE SYMBOL NM

87-0222 *Nachman*

AFOSR-TR. 89-0433

**THREE-DIMENSIONAL MODELLING FOR
CONTACT RESISTANCE OF CURRENT FLOW
INTO A SOURCE/DRAIN REGION**

Ellis Cumberbatch
and
Weifu Fang

Mathematics Department
The Claremont Graduate School
Claremont, CA 91711

Approved for public release
distribution unlimited.

Abstract

Various extensions of the transmission line model are introduced to find the resistance for current flow in MOSFET source/drain regions. The geometry is taken to be a rectangular box with a rectangular contact on the upper surface. Explicit formula are derived by assuming that the current flow is restricted to various geometrical planes. Comparison of basic results with simulation and experimental data is good. Comparison with simulation results for misalignment is less good.



Accession For	
NTIS CRA&I	<input checked="" type="checkbox"/>
DTIC TAB	<input type="checkbox"/>
Unannounced	<input type="checkbox"/>
Justification	
By	
Distribution /	
Availability Codes	
Dist	Avail and/or Special
A-1	

Acknowledgement

This work originated in project work done for the Jet Propulsion Laboratory by The Claremont Graduate School Mathematics Clinic. The continued encouragement and advice of Cesar Pina, Martin Buehler and Udo Lienewig of the JPL VLSI group is gratefully acknowledged. This work was supported by the U.S. Air Force Office of Scientific Research under grant AFOSR - 87-0222.

I. Introduction

Various models have been suggested in attempts to find resistance formulae for current flow in source/drain regions of metal-oxide-semiconductor field-effect transistors (MOSFET's). This parasitic resistance becomes relatively more important under device miniaturization, and its dependence on geometrical and physical parameters is sought. Measurement of resistance across single contacts ([1],[2]) indicate large variability neighbor to neighbor. This portends the use of statistics in estimating the yield of a device, [3], and it has implications for the quality control of the fabrication process. Some of the variability is random, due, say, to the imperfect removal of photo-resist, but some has global features. Chief of the latter derive from misalignment: contact regions have been etched in non-symmetrical locations. In order to estimate the effects of contact size and location some two and three dimensional models are constructed here, resulting in resistance formulae of varying complexity. Results for typical parameter ranges are compared with simulation and with test data.

The simplest model, the transmission line model (TLM), [4], [5], is one-dimensional as it neglects both width and depth variations. Improvements on the TLM have been provided in [6], where depth dependence was included, and in [7]-[9], where modelling of contact width and side tabs was presented.

The physical set-up is shown in Figure 1. The source/drain region is taken to be a rectangular block of width w , depth t . The contact is rectangular of length b , width w_c , and has flange distances w_1, w_2, c from the source/drain boundary, as shown.

Current, uniformly distributed across the end surface S , flows along the block and exits across the contact. The electrostatic potential, ϕ , satisfies a zero normal derivative boundary condition on bounding surfaces except on S , and except on the contact where an ohmic interfacial resistance holds. This gives rise to the boundary condition

$$(1.1) \quad \phi_y - \tau\phi = 0 \text{ on the contact}$$

$$\text{where } \tau = 1/(\sigma\rho_c).$$

Here σ is the material conductivity and ρ_c the contact resistivity.

The models developed in this paper are extensions of the TLM, and of the work done in [6]. Model 0 assumes that current enters the contact only from a region directly upstream of the contact, and uses the TLM formula. Model I adds to this the contribution of the flanges. Model II is fully three-dimensional, extending the analysis in [6]. The key assumption is to prescribe that current lines remain on planes parallel to the edges of the box. Current flow between two adjacent planes is then two-dimensional, and the full result is achieved by integration in the third direction. Models III and IV are variants of II taking into account different current distributions.

II. Models for contact resistance

Model 0 For a contact of width w_c the series or front resistance, R_F , is given by the TLM

$$(2.1) \quad \text{as } R_s/R_F = (w_c/L) \tanh(b/L), \quad \text{where } L = (t\sigma\rho_c)^{1/2}$$

and $R_s = \rho_c/L^2$ is the sheet resistance of the material. Substitution of \sinh for \tanh in (2.1) yields the end resistance, R_{END} . Model 0 involves neither the flange widths w_1, w_2 nor the depth t (except as in L). The models introduced below account for these thickness and flange effects. As a result, Model 0 cannot be compared properly in the graphs presented. It is quoted only to introduce the formula (2.1).

Model I The flanges are assumed to generate additional (parallel) resistance, computed by viewing the flange regions as having width t and depths w_1, w_2 . However, poor results from this at small values of w_c (where $R_F \sim w_c^{-2}$ is expected) made us reflect on the current flow interactions. The current lines squeezing in from the flange regions are competing with the center current lines which have depth t . Details of the current flowing in from the sides will not be felt by the contact until that current is at a similar distance from the side edge of the contact. Consequently (and after some experimentation) the flange regions were taken to have depths t_1, t_2 where

$$(2.2) \quad t_1 = \min(w_1, t) , t_2 = \min(w_2, t).$$

The front resistance is then given by

$$R_s/R_F = (w_c/L) \tanh(b/L) + (w_1/L_1) \tanh(w_c/L_1) + (w_2/L_2) \tanh(w_c/L_2)$$

(2.3) where $L_i = (t_i \sigma \rho_c)^{1/2}$, $i = 1, 2$.

Model II This is an attempt to construct a three-dimensional approximation to current flow in the complicated geometry of Figure 1. The main assumption is that current lines remain on planes parallel to the x-axis (the planes are not parallel to each other). The planes, and the reduction of the three-dimensional problem to a sequence of two-dimensional ones, are found by the following two prescriptions.

Prescription (1): Consider the end surface S and a line through $z = r$. The line divides S into two areas. See Figure 2. Consider the plane defined by extending this line parallel to the x-axis. The assumption that current lines do not cross such planes implies that current entering area A exits on the portion of the contact on $w_1 < z < r$. The geometrical relation

$$(2.4) \quad (r - w_1)/w_c = A/\text{area of } S = A/tw$$

is taken to define the plane through $z = r$. It follows that there is a point r_0 where the area A becomes rectangular, of area $A = r_0 t$. Hence (2.4) gives

$$(2.5) \quad r_0 = ww_1/(w - w_c).$$

It is now permissible to concentrate only on the portion of the source/drain region defined by $0 < r < r_0$, as the remaining portion will have the same characteristics under this model, and its resistance can be found by appropriate substitutions. For the rectangle defined by $0 < r < r_0$ the plane passing through the corner $y = t, z = 0$, occurs at $r = r^*$, say, where

$$(2.6) \quad r^* = 2ww_1/(2w - w_c).$$

(See Figure 3). Planes through $z = r$ for $r^* < r < r_0$ intersect the bottom of the region, giving an intercept $h(r)$ and a plane depth $\epsilon_1(r)$ where

$$(2.7) \quad h = [r(2w - w_c) - 2ww_1]/w_c,$$

$$(2.8) \quad \epsilon_1^2 = t^2 + 4[ww_1 - r(w - w_c)]^2/w_c^2,$$

whilst planes through $z = r$ for $w_1 < r < r^*$ intersect the side of the region with intercept $p(r)$ and plane depth $\epsilon_2(r)$ given by

$$(2.9) \quad p = 2tw(r - w_1)/(rw_c),$$

$$(2.10) \quad \epsilon_2^2 = r^2 + 4t^2w^2[1 - w_1/r]^2/w_c^2.$$

Prescription (2): Consider an area element formed between the planes $z = r$ and $z = r + dr$.

These are shown in Figure 4 for the cases $r^* < r < r_0$ and $w_1 < r < r^*$.

The area elements are replaced by the sector area element shown in Figure 4(c), of equal area. Note that, from (2.4),

$$(2.11) \quad dA = (wt/w_c)dr.$$

The current flow in an area element is now assumed to take place in the sector element of Figure 4(c), and the equation to be solved is Laplace's equation in cylindrical coordinates, assuming angular independence. The analysis for this is given in the Appendix. The resistance for the element dA given in (A.37) is integrated over S to give R_F as

$$(2.12) \quad R_s/R_F = \frac{1}{L} \cdot \sqrt{\frac{w}{w_c}} \left\{ \int_{r^*}^{r_0} \sqrt{\frac{t}{\epsilon_1}} \tanh \left(\sqrt{\frac{t}{\epsilon_1} \cdot \frac{w_c}{w} \cdot \frac{b}{L}} \right) dr \right. \\ \left. + \int_{w_1}^{r^*} \sqrt{2 \frac{r-w_1}{r} \cdot \frac{t}{\epsilon_2} \cdot \frac{w}{w_c}} \tanh \left(\sqrt{2 \frac{r-w_1}{r} \cdot \frac{t}{\epsilon_2} \cdot \frac{b}{L}} \right) dr \right\}$$

where ϵ_1, ϵ_2 are given in (2.8). Note that the result (2.12) is for resistance in the region $0 < r < r_0$. If the contact is symmetrically placed, $r_0 = w/2$, and R_s/R_F for the whole device will be twice that of (2.12); if not, the expression (2.12) has to include a similar expression obtained by replacing w_1 by w_2 .

Model III Prescription (1) of Model II implies that an element dr of the contact width is proportional to dA , an element of S , see (2.11). Since current is uniformly distributed across S this means that equal elements of the contact receive equal

amounts of current; that is, the current density is uniform across the contact width. However a non-uniform distribution is expected as current entering from the flanges will be confined to a layer close to the sides. An estimate of the non-uniformity is provided by the TLM, that is by Model I. The current density for the region defined the contact, i.e., $w_1 < r < r_0$, is taken as uniform. The current coming from the flange, $0 < r < w_1$, is estimated by the TLM, as proportional to

$$(2.13) \quad \frac{w_1}{L_1} \cosh\left(\frac{r-r_0}{L_1}\right) \left\{ \sinh\left(\frac{r_0-w_1}{L_1}\right) \right\}^{-1} \text{ for } w_1 < r < r_0$$

Combining these yields the replacement

$$(2.14) \quad dA = t \left[1 + \frac{w_1}{L_1} \cosh\left(\frac{r-r_0}{L_1}\right) \left\{ \sinh\left(\frac{r_0-w_1}{L_1}\right) \right\}^{-1} \right] dr$$

for (2.11), and an appropriate change in the formula for R_F in (2.12). Also the calculation for r^* is changed to the solution to

$$(2.15) \quad r^* = 2w_1 K(r^*)$$

$$\text{where } K(r) = \sinh\left(\frac{r_0-r}{L_1}\right) \left\{ \sinh\left(\frac{r_0-w_1}{L_1}\right) \right\}^{-1}$$

Similar changes are made for the current contribution from the flange w_2 .

Model IV The introduction in Model III of a relation between dA and dr which is non-uniform also gives A as a function of r (by integrating (2.14)) different from

(2.4). There follows new formulae for ϵ_1, ϵ_2 viz.

$$\epsilon_1^2 = t^2 + 4w_1^2 K^2(r) \quad , \quad \epsilon_2^2 = r^2 + 4t^2 \left\{ 1 - \frac{w_1}{r} K(r) \right\}^2$$

which are incorporated in Model IV.

III. Results Various results derived from the formula (2.12) and the corresponding ones from Models III and IV are shown in Figures 7 to 10. In the TLM the thickness t is parametrically involved only in the definition of L and this carries over to most simulations as the latter are derived from the numerical solution of two-dimensional partial differential equations (in $z = 0$). Loh et al, [9], have carried out some three-dimensional simulations and show differences between 1-D, 2-D, and 3-D results for R_k , the Kelvin resistance, which is not appropriate for the model constructed here. There are more simulations for the 2-D case and we use these for comparison. However we note that

- (1) we are comparing different models, and
- (2) as is evident from formula (2.12), and as noted in [9], Appendix, the thickness t enters the 3-D models as a parameter to be chosen in relation to the other length scales w_1, w_c, L . As a consequence we can vary t to see its effect on the results.

Figures 7 (a) - (d) show $\log(R_F/R_s)$ versus $\log(w_c/w_1)$ for $L/w_1 = .358$ for Models I-IV for $t/w_1 = .1, .5, 1, 10$ respectively. Simulation data from [9], Figure 12, is also shown. It is noted that $t/w_1 = .5, 1, 10$ give good comparisons, indicating some insensitivity to t over this range. As above we note that we are comparing different models. Figures 8 (a) - (d) repeat the same results for the case $L/w_1 = .567$.

Figure 9 shows $\log(R_E/R_s)$ versus $\log(w_c/w_1)$ plus simulations from [9], Figure 11, for $t/w_1 = 1$ and for $L/w_1 = .567$ (upper curve), $L/w_1 = .358$ (lower curve). These show reasonable comparisons.

Results relevant to misalignment estimates are shown in Figure 10, where also are drawn the simulation data of [10].

IV. Comments

There are small differences between the results presented here and the simulations in Figures 7,8,9 and substantial ones in those of Figure 10. Apart from the fact that R_{END} is more volatile than R_F , there are significant differences in the approaches, which bear comment.

The 2-D simulations are based on solving

$$(4.1) \quad \begin{aligned} L^2 \nabla^2 \phi &= \phi && \text{on the contact,} \\ \nabla^2 \phi &= 0 && \text{off it} \end{aligned}$$

by numerical methods over the plane $z = 0$, imposing a constant voltage upstream at a station such as S . This turns out to be equivalent to the TLM. A derivation of (4.1) based on averages across a thin layer is given in [9]. An alternative is as follows. Note that the boundary-value problem posed by (1.1) is equivalent to minimizing the integral

$$(4.2) \quad J = \int_{\text{volume}} |\nabla \phi|^2 dv + \tau \int_{\text{contact}} \phi^2 dS.$$

Now assume at small t that the volume integral may be approximated by t times the surface integral and assume that the τ term applies only on the contact. The zero variation of J yields (4.1). We remark in passing that numerical simulations based on (4.2) may be more efficient than 3-D finite difference schemes.

The work in [6] improved the TLM to account for depth effect (to first order). It showed

- (a) that (4.1) must be supplemented by a transition layer of width L on either side of the contact boundary. A more complicated boundary value problem holds in this layer.
- (b) that the effect of including depth is substantial on R_{ENV} , less so on R_F .

The formulae presented in Section II do not include the depth effects calculated in [6]. The latter could be included: easily in Model I; approximately, and at the expense only of more complicated formula, in Models II-IV. However the models presented do take into account the fact that current lines have a three-dimensional trajectory, and it is argued that they may be more realistic than simulations based on (4.1) which is a two-dimensional approximation.

The divergences between the two approaches as seen in Figure 10 suggest that the modeling is inappropriate for misalignment effects in one or both the approaches. The modelling here assumes current flow along planes parallel to the x-axis. As a consequence the formulae derived involve the contact length b as an argument. In practice, current lines, on approach to a square contact, may react to the proximity of contact side edges as well as the rear edge, thereby reducing b in the argument. This effect shows more dramatically in R_{EVD} which evaluates \sinh of arguments than in R_F which evaluates \tanh .

APPENDIX

We wish to solve Laplace's equation in cylindrical coordinates, with no angular variation. That is

$$(A.1) \quad \partial^2 \phi / \partial r^2 + (1/r) \partial \phi / \partial r + \partial^2 \phi / \partial x^2 = 0$$

for the boundary value problem shown in Figure 5. The sector occupies the region $r_1 < r < r_2$ and $-\infty < x < \infty$. (The source/drain boundary at $x = -(b+c)$ is removed in this analysis as its effect on the results is assumed to be weak. An approximation which corrects for this omission can be introduced without difficulty). The sector depth

$$(A.2) \quad \epsilon = r_2 - r_1$$

is assumed to be small, and an asymptotic result based on $\epsilon \ll 1$ similar to the analysis for the plane case presented in [6] is obtained. That analysis was predicated on the existence of boundary layer solutions in regions close to the ends of the contact, i.e. on planes $x = 0$ and $x = -b$. Consequently there are five regions where separate solutions are found (see Figure 6), and these solutions are joined in the conventional approach of the method of matched asymptotic expansions ([11] or [12]). Solutions for the five regions are as follows:

Region I: This region contains no current lines and the potential is constant. Hence

$$(A.3) \quad \phi = \alpha + \epsilon r \beta + \dots,$$

where α, β are constants to be found subsequently.

Region II: In terms of scaled variables for the region near the contact end

$$(A.4) \quad m = (x + b)/\epsilon, \quad n = (r - r_1)/\epsilon,$$

an asymptotic expansion for the solution is

$$(A.5) \quad \phi = \alpha + \epsilon\tau[\beta + \alpha\phi_1(m, n)] + \dots$$

The perturbation potential, ϕ_1 , satisfies boundary conditions

$$(A.6) \quad \begin{aligned} \partial\phi_1/\partial n = 0 & \quad \left\{ \begin{array}{l} \text{on } n = 0, m < 0 \\ \text{on } n = 1, \text{ all } m \end{array} \right. \\ \text{and } \partial\phi_1/\partial n = 1 & \quad \text{on } n = 0, m > 0. \end{aligned}$$

In the plane case, [6], an explicit integral expression was found for ϕ_1 ; here a series expansion is obtained.

In $m < 0$

$$(A.7) \quad \phi_1 = \sum_N e^{Nm} F_N(s) \quad \text{where } s = n + r_1/\epsilon,$$

$$(A.8) \quad \text{and where } F_N'' + (1/s)F_N' + N^2 F_N = 0.$$

Hence

$$(A.9) \quad F_N = A_N J_0(Ns) + B_N Y_0(Ns).$$

The boundary conditions that $F_N = 0$ on $n = 0$ and $n = 1$ determine the eigenvalues N and the ratios $A_N : B_N$. The purposes for which we require the solution do not require us

to complete this part of the calculation.

In $m > 0$

The condition that the boundary condition (A.6) yields the correct current exiting the contact implies that ϕ_1 is $O(m^2)$ as $m \rightarrow \infty$, and that

$$(A.10) \quad \phi_1 = k_1[m^2 - s^2/2] + k_2 \ln s + k_3 + \sum_N e^{-Nm} G_N(s),$$

$$(A.11) \quad \text{where} \quad k_1 = \epsilon r_1 / (r_2^2 - r_1^2), \quad k_2 = r_1 r_2^2 / \epsilon (r_2^2 - r_1^2).$$

The solution for the eigenfunctions G_N is as in (A.9) with constants again determined (in ratio) by the boundary conditions. The continuity of ϕ_1 and $\phi_{1,m}$ across $m = 0$ is required to supply sufficient conditions to fix the constants in (A.9) and similar ones in (A.10). There remains the constant k_3 in (A.10) to be determined. In the plane case, [6], this constant was determined as a consequence of the availability of an exact result. However it was noticed there that the constant could also be determined from the physical principal that the average potential increase in the x-direction is a consequence of current flow across the contact. This latter condition is invoked here and gives

$$(A.12) \quad k_3 = (r_1/4\epsilon\Delta^2) \left\{ (1 + r_1/\epsilon)^4 - (r_1/\epsilon)^4 \right\} \\ - 2(1 + r_1/\epsilon)^2 \left[2(1 + r_1/\epsilon)^2 \ln(1 + r_1/\epsilon) - 2(r_1/\epsilon)^2 \ln(r_1/\epsilon) - \Delta \right]$$

$$(A.13) \quad \text{where} \quad \Delta = (1 + r_1/\epsilon)^2 - (r_1/\epsilon)^2$$

Note that the series terms in (A.10) are exponentially decreasing as x increases into the contact region, and the non-series terms carry the dominant information concerning the current flow to be matched with the solution in Region III.

Region III: The scaling relevant here is

$$(A.14) \quad \xi = (\tau/\epsilon)^{1/2}x, \quad \eta = (r - r_1)/\epsilon.$$

The analysis is a little more sophisticated than that for Region II, so we present more of the details. The differential equation (A.1) becomes

$$(A.15) \quad \phi_{\eta\eta} + \phi_{\eta}/(\eta + r/\epsilon) = -\tau\epsilon\phi_{\xi\xi},$$

and the boundary condition (2.1) becomes

$$(A.16) \quad \phi_{\eta} = \tau\epsilon\phi.$$

The asymptotic series is taken as

$$(A.17) \quad \phi = \phi_0 + \epsilon\tau\phi_1 + \epsilon^2\tau^2\phi_2 + \dots$$

so that the first two terms satisfy

$$(A.18) \quad \phi_{0\eta\eta} + a\phi_{0\eta}/(\eta + r_1/\epsilon) = 0$$

with boundary conditions

$$(A.19) \quad \phi_{0\eta} = 0 \quad \text{at } \eta = 0 \text{ and } \eta = 1,$$

$$(A.20) \quad \text{and} \quad \phi_{1\eta\eta} + \phi_{1\eta}/(\eta + r_1/\epsilon) = -\phi_{0\xi\xi},$$

with boundary conditions

$$(A.21) \quad \phi_{1\eta} = \phi_0 \text{ at } \eta = 0, \text{ and } \phi_{1\eta} = 0 \text{ at } \eta = 1.$$

The solution of (A.17) and (A.18) is

$$(A.22) \quad \phi_0 = M(\xi)$$

and that of (A.19)

$$(A.23) \quad \phi_1 = M''(\eta + r_1/\epsilon)^2/4 + N(\xi)\ln(\eta + r_1/\epsilon) + P(\xi),$$

with boundary conditions (A.21) giving

$$(A.24) \quad N\epsilon/r_1 - M''r_1/2\epsilon = M$$

$$\text{and} \quad N/(1 + r_1/\epsilon) - M''(1 + r_1/\epsilon)/2 = 0$$

Hence, eliminating N ,

$$(A.25) \quad M''\Delta = M2r_1/\epsilon$$

The solution of (A.25) which matches with the leading term from (A.10) for Region II gives

$$(A.26) \quad \phi_0 = \alpha \cosh[\mu(\xi + \Gamma)]$$

$$(A.27) \quad \text{where} \quad \Gamma = (\tau/\epsilon)^{1/2}b, \quad \mu = (2r_1/\epsilon\Delta)^{1/2}.$$

The solution for ϕ_1 is found in similar fashion:

$$(A.28) \quad \phi_1 = (1/2)\alpha\mu^2\{(1+r_1\epsilon)^2\ln(\eta+r_1/\epsilon) - (\eta+r_1/\epsilon)^2/2\} \cosh\mu(\xi+\Gamma) \\ + k_4\alpha(\xi+\Gamma) \sinh\mu(\xi+\Gamma) + (\beta + \alpha k_3) \cosh\mu(\xi+\Gamma),$$

where

$$(A.29) \quad \Delta k_4 = \mu^3[(1+r_1/\epsilon)^4 - (r_1/\epsilon)^4]/16 - \mu(r_1/\epsilon)^3/4 \\ - \mu^3(1+r_1/\epsilon)^2[(1+r_1/\epsilon)^2\ln(1+r_1/\epsilon) - r_1/\epsilon)^2\ln(r_1/\epsilon) - \Delta/2]4 \\ + (1/\mu\Delta)(r_1/\epsilon)^2(1+r_1/\epsilon)^2\ln(r_1/\epsilon)$$

Region IV: The scaling used near the contact leading edge is

$$(A.30) \quad p = x/\epsilon, \quad q = (r - r_1)/\epsilon.$$

Matching with the solution from Region III indicates that a series in powers of $(\epsilon)^{1/2}$ is required, and the solution is developed as

$$(A.31) \quad \phi = \alpha \cosh \mu\Gamma + (\tau\epsilon)^{1/2}\alpha\mu p \sinh \mu\Gamma + \tau\epsilon\phi_2(p, q) + \dots$$

Here ϕ_2 is harmonic and satisfies the boundary conditions

$$(A.32) \quad \partial\phi_2/\partial q = 0 \left\{ \begin{array}{l} \text{on } q = 0, p > 0 \\ \text{on } q = 1, \text{ all } p, \end{array} \right.$$

$$\text{and} \quad \partial\phi_2/\partial q = \alpha \cosh \mu\Gamma \text{ on } q = 0, p < 0.$$

The solution for ϕ_2 is

$$(A.33) \quad \phi_2 = \alpha k_4 \Gamma \sinh \mu \Gamma + \{\beta + \alpha k_3 + \alpha \mu^2 [p^2/2 - (q + r_1/\epsilon)^2/4 + (1/2)(1 + r_1/\epsilon)^2 \ln(q + r_1/\epsilon)]\} \cosh \mu \Gamma + \alpha \sum_N e^{-Np} H_N(q + r_1/\epsilon) \quad \text{for } p < 0,$$

and

$$\phi_2 = (\beta + \alpha k_3) \cosh \mu \Gamma + k_4 \alpha \Gamma \sinh \mu \Gamma + \alpha \sum_N e^{-Np} I_N(q + r_1/\epsilon) \quad \text{for } p > 0.$$

The terms H_N, I_N in the infinite series above are linear combinations of Bessel functions and are evaluated in a similar fashion to those in the Region II solutions. However, their exact nature is not required.

Region V: The asymptotic behaviour of the Region IV solution as $p \rightarrow \infty$ provides the solution here. This is found to be

$$(A.34) \quad \phi = (\tau/\epsilon)^{1/2} x \alpha \tau \sinh \mu \Gamma + \alpha \cosh \mu \Gamma + \tau \epsilon \{(\beta + \alpha k_3) \cosh \mu \Gamma + (1/2) k_4 \alpha \Gamma \sinh \mu \Gamma\} + \dots$$

The first term in (A.34) represents the uniformly distributed current.

This completes the analysis for generating and matching the solutions in Regions I-V. The constants α, β assumed for the solution in Region I, equation (A.3), may now be specified. If the total current in Region V is I , and the cross-sectional area is S , the current density is I/S . Equating this with $\sigma \partial \phi / \partial x$ from (A.34) yields

$$(A.35) \quad \alpha = (I/S) \{ \sigma (\tau/\epsilon)^{1/2} \mu \sinh \mu \Gamma \}^{-1}.$$

$$(A.36) \quad \beta = -\frac{k_1 \Delta \alpha}{4r_1} (1 + \mu \Gamma \coth \mu \Gamma)$$

The resistance of an element dS may now be calculated. The end resistance is related to the potential at $x = -b$, and the front resistance to that at $x = 0$. Hence

$$(A.37) \quad \begin{aligned} R_{END} &= (\alpha + \epsilon \tau \beta + \dots) / \left(\frac{I}{S} dS \right) \\ &= \{ \sigma (\tau / \epsilon)^{1/2} \mu \sinh \mu \Gamma dS \}^{-1} \end{aligned}$$

to first order. Likewise R_F has a similar form, replacing \sinh by \tanh .

References:

1. U. Lieneweg and D. Hannaman, "Yield Analysis of Interfacial Contact Resistance Measurements on Cross Contact Chain," IEEE VLSI Workshop on Test Structures, Long Beach, CA (1986) Digest p. 252.
2. M. Buehler and H. Sayah, "Contact Resistance Measurements Using an Addressable Array," Presented at the VLSI Multilevel Interconnection Conference, June 1987.
3. H. Heijmans, et.al., "Analysis of Resistances in the Cross Contact Chain," The Claremont Graduate School Mathematics Clinic Report, 1987.
4. H. Murrman and D. Widmann, "Current Crowding on Metal Contacts to Planar Devices," IEEE Trans. Electron Devices, vol. ED-16, p. 1022, 1969.
5. H. H. Berger, "Models for Contacts to Planar Devices," Solid-State Electron, vol. 15, p. 145, 1972.
6. J. Pimbley, E. Cumberbatch, and P. S. Hagan, "Analytical Treatment of MOSFET Source-Drain Resistance," IEEE Trans. Electron Devices, vol. ED-34, No. 4, April, 1987.
7. U. Lieneweg and D. Hannaman, "New Flange Correction Formula Applied to Interfacial Resistance Measurements of Ohmic Contacts to GaAs," IEEE Electron Device Letters EDL-8, p. 202 (1987)
8. T. Schreyer and K. Saraswat, "A Two-Dimensional Analytical Model of the Cross-Bridge Kelvin Resistor," IEEE Electron Device Letters, Vol. EDL-7, No. 12, December 1986.
9. W. M. Loh, S. E. Swirhern, T. A. Schoeyer, R. M. Swanson, K. C. Saraswat, "Modeling and Measurement of Contact Resistances," IEEE Trans. Electron Devices, Vol. ED-34, No. 3, March 1987.
10. A. Scorzoni, M. Finetti, K. Graham, I. Suni and P. Cappell, "Current Crowding and Misalignment Effects as Sources of Error Contact Resistivity Measurements," IEEE Trans. Electron Devices, Vol. ED-34, No. 3, March 1987
11. J. Kevorkian and J. D. Cole, Perturbation Methods in Applied Mathematics. New York: Springer-Verlag, 1981.
12. A. H. Nayfeh, Perturbation Methods, John Wiley & Sons, 1973.

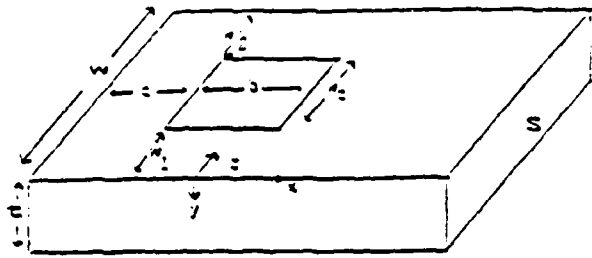


FIGURE 1 Physical set-up.

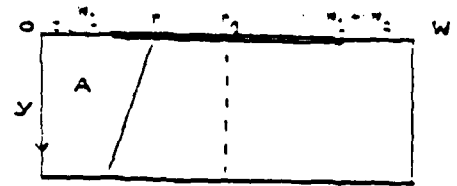


FIGURE 2 End surface S.

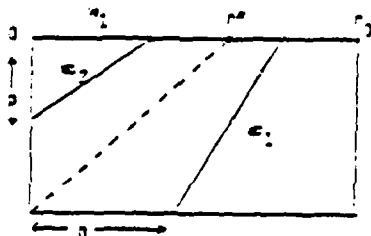


FIGURE 3 End surface for $0 < z < r_0$

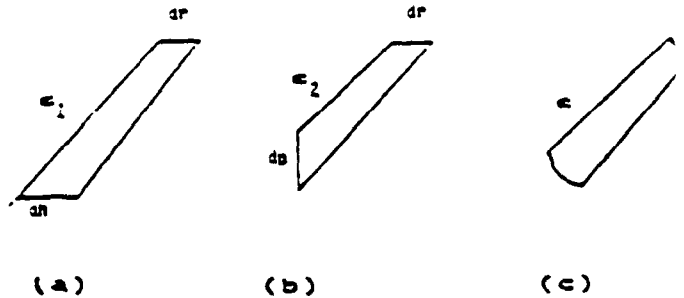


FIGURE 4

- (a) Area element for $r_1 < r < r_2$
- (b) Area element for $w_1 < r < r_2$
- (c) Replacement element

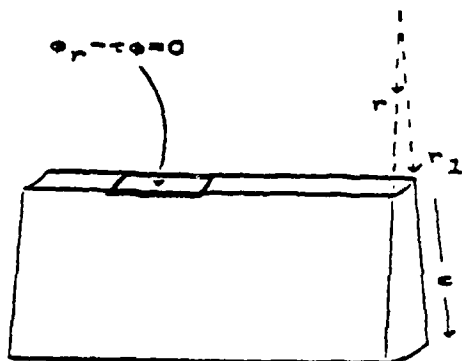


FIGURE 5 Boundary value problem.

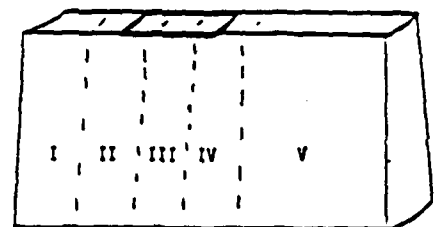


FIGURE 6 Regions for separate asymptotic expansions.

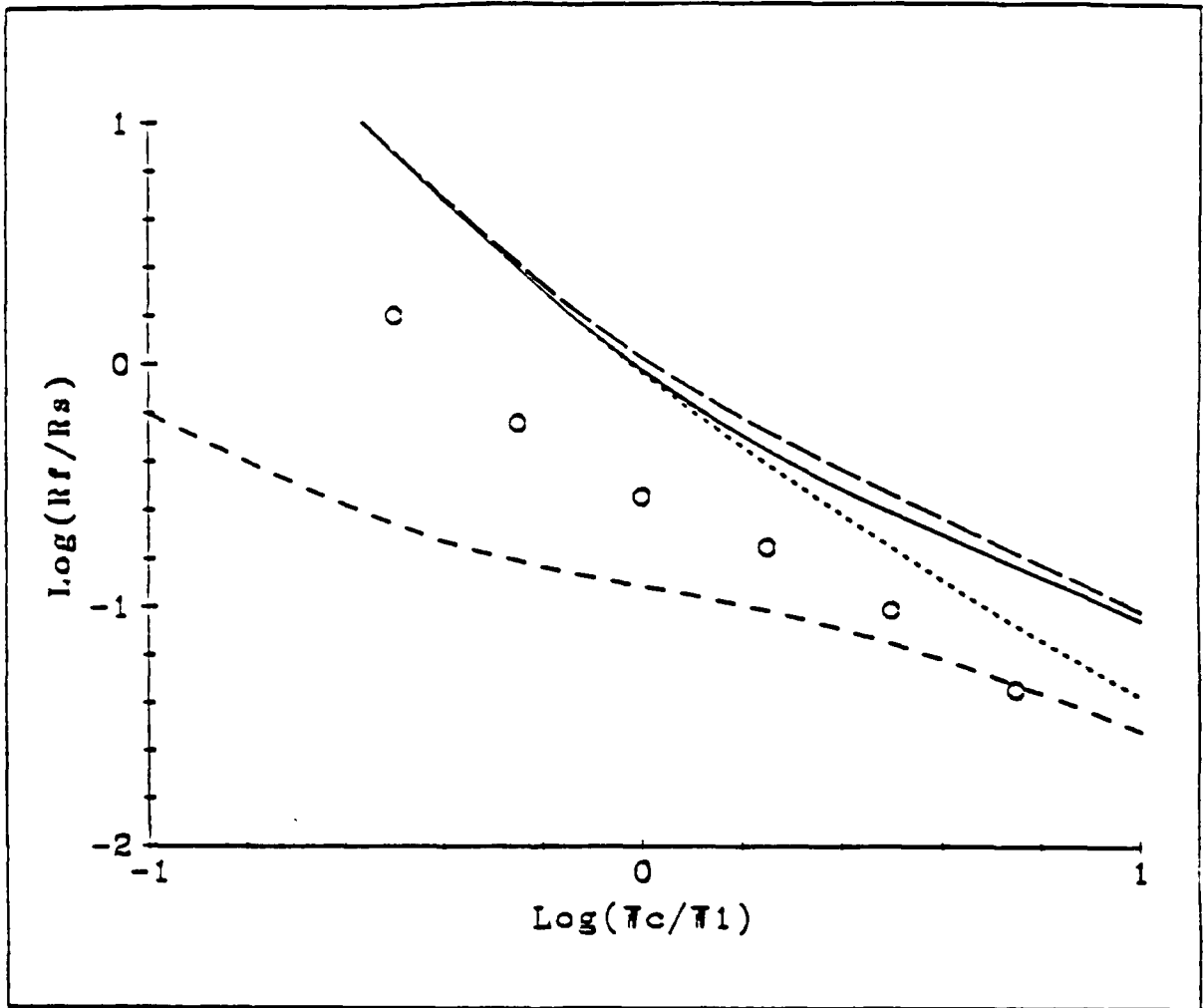
Legend

Figures 7 (a) - (d) Graphs of $\log(R_F/R_s)$ versus $\log(w_c/w_1)$ for Models I, II, III, IV, for $t/w_1 = .1, .5, 1, 10$, respectively, plus simulation data from [9]. The graphs may be interpreted as keeping t and w_1 fixed and varying w_c .

Figures 8(a) - (d) Same as Figure 7 with $L/w_1 = .567$.

Figure 9 Graph of $\log(R_{END}/R_s)$ versus $\log(w_c/w_1)$ for $t/w_1 = 1$ and for $L/w_1 = .567$ (upper curve), $L/w_1 = .358$ (lower curve).

Figure 10 Graph of R_E versus w_1 to show the effect of misalignment. The results are for a square contact with $w_c = 5\mu m$ and $R_s = 20\Omega/\square$ and for $t = .5, 1\mu m$. The simulation data is taken from [10], Figure 4.

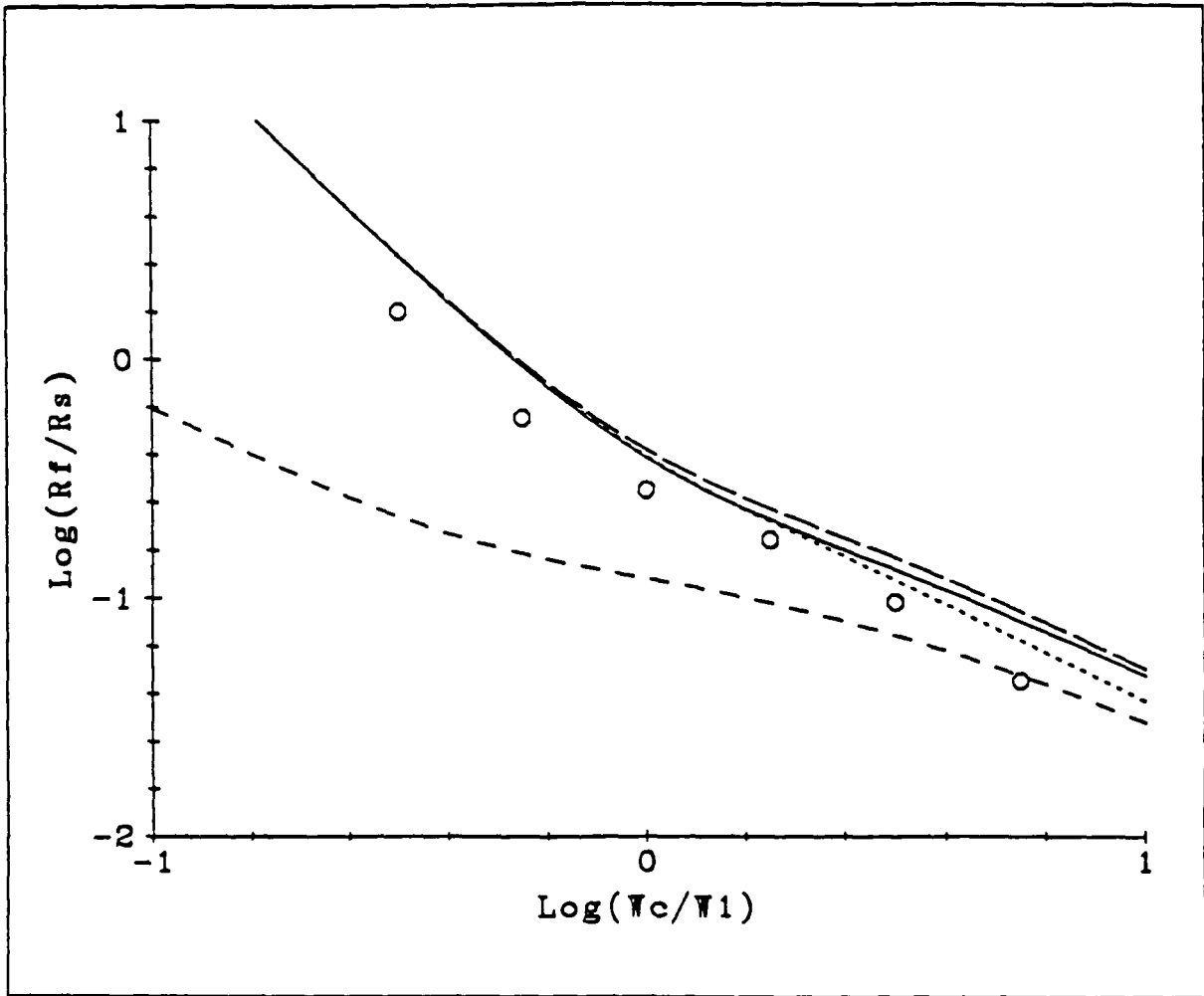


- - - - - Model I
 ————— Model II
 - · - · - Model III
 ········· Model IV
 ○ ○ ○ ○ Simulation Data

$L/W_1 = 0.358$

$t/W_1 = 0.1$

FIGURE 7a

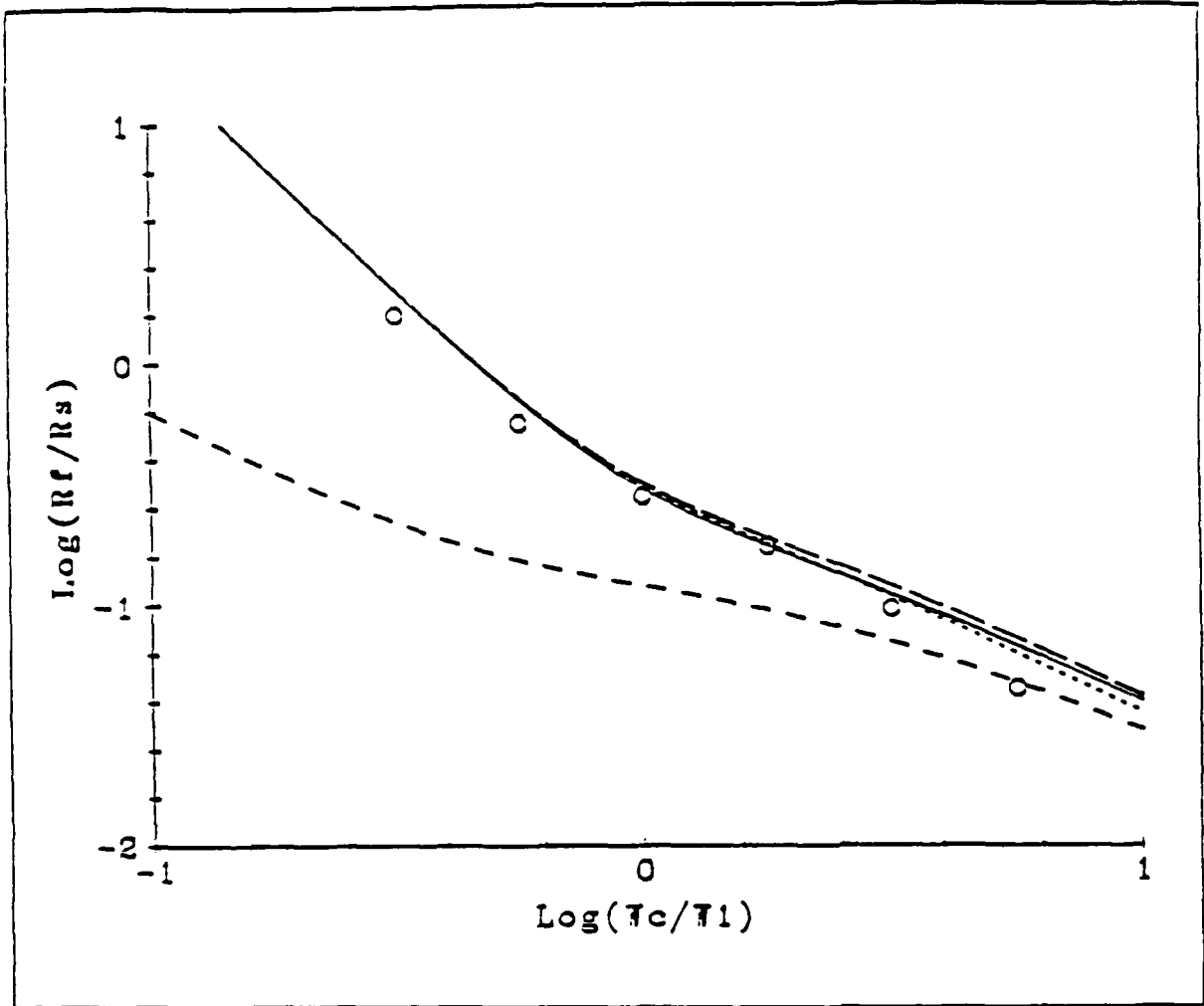


- - - - - Model I
 _____ Model II
 - . - . - . Model III
 Model IV
 O O O O Simulation Data

$L/W1=0.358$

$t/W1=0.5$

FIGURE 7b

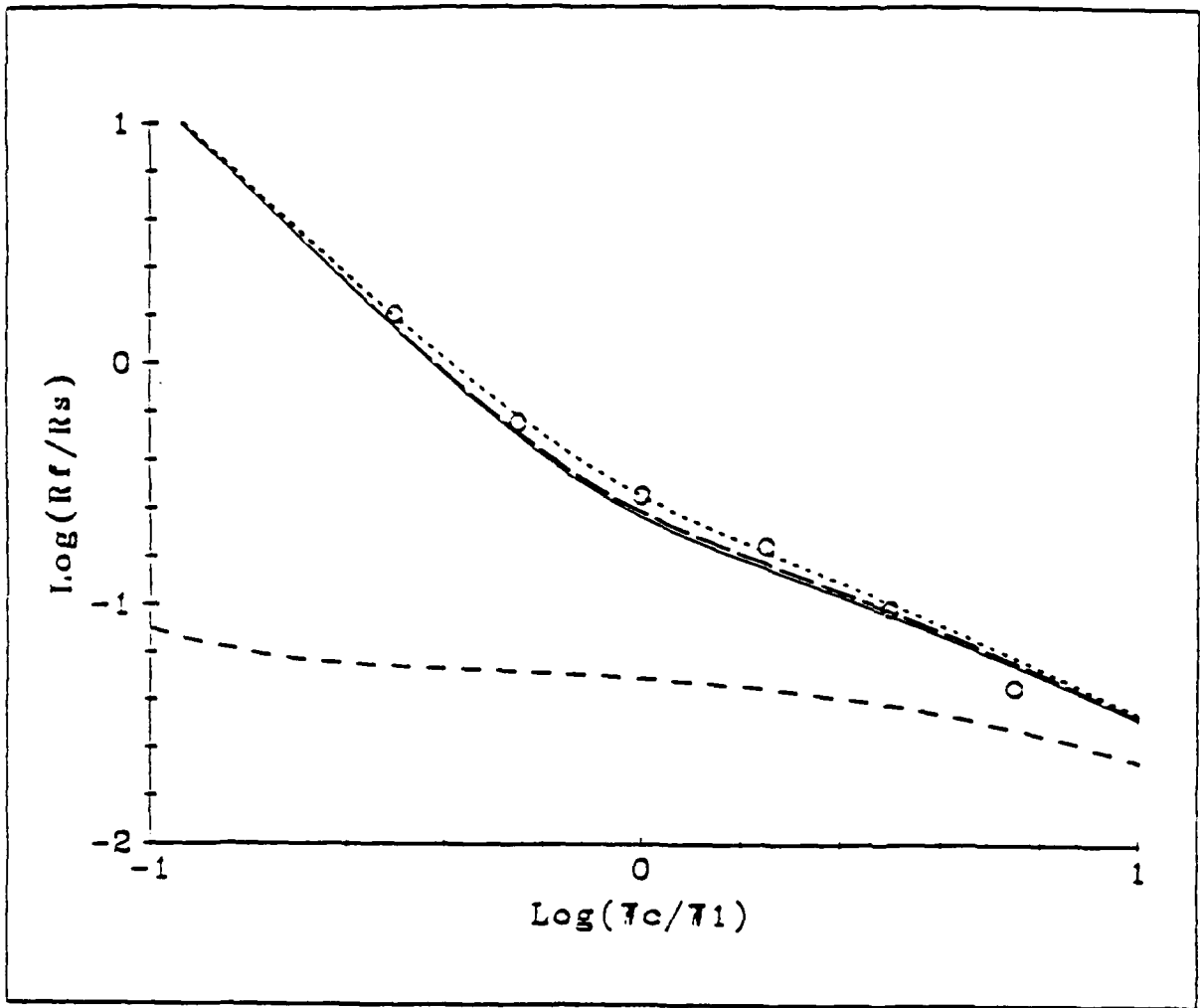


- Model I
- Model II
- · - · - Model III
- Model IV
- ○ ○ ○ Simulation Data

$L/W1=0.358$

$t/W1=1.0$

FIGURE 7c

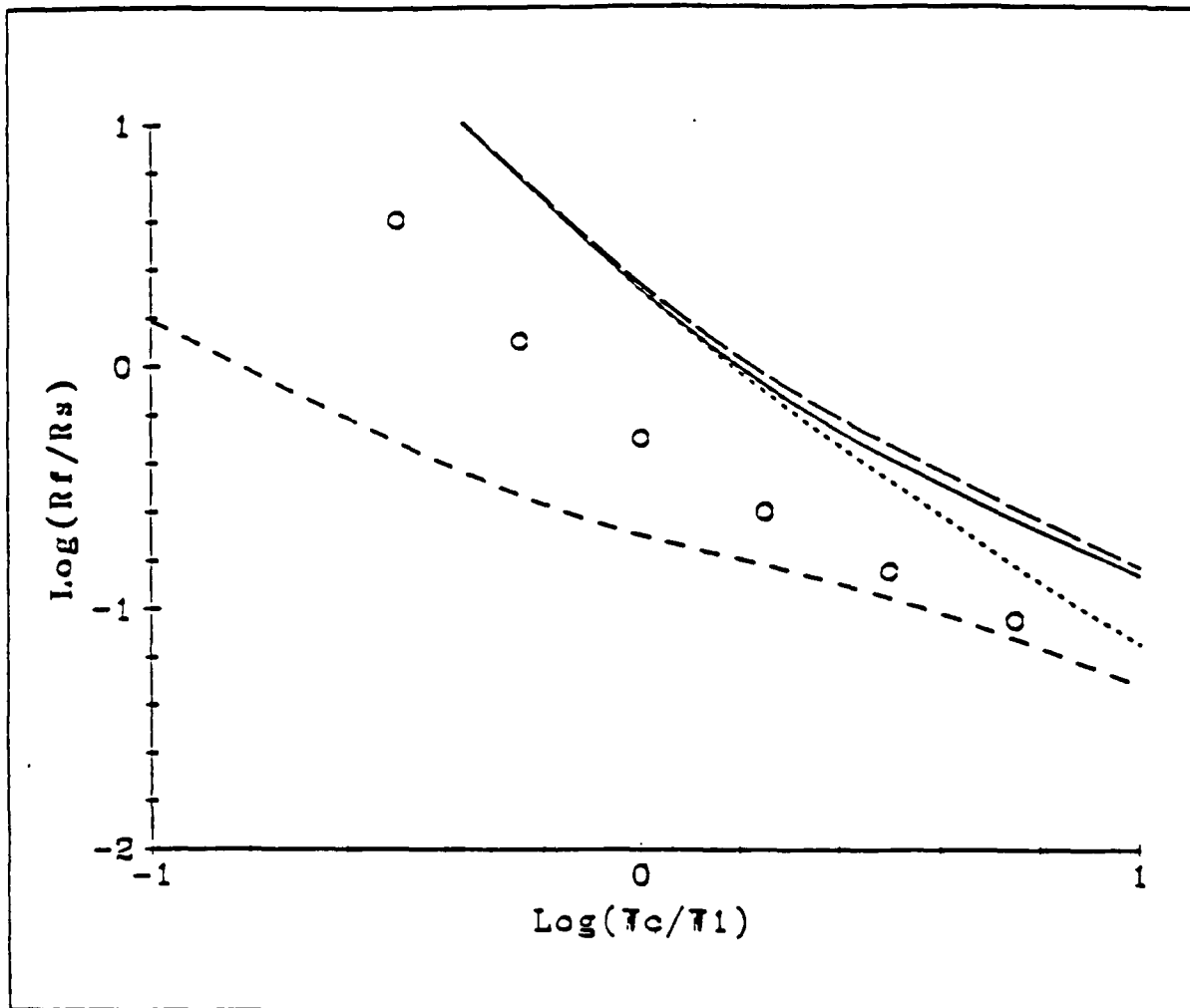


- - - - - Model I
 ————— Model II
 - - - - - Model III
 Model IV
 O O O O Simulation Data

$L/W_1 = 0.358$

$t/W_1 = 10.0$

FIGURE 7d

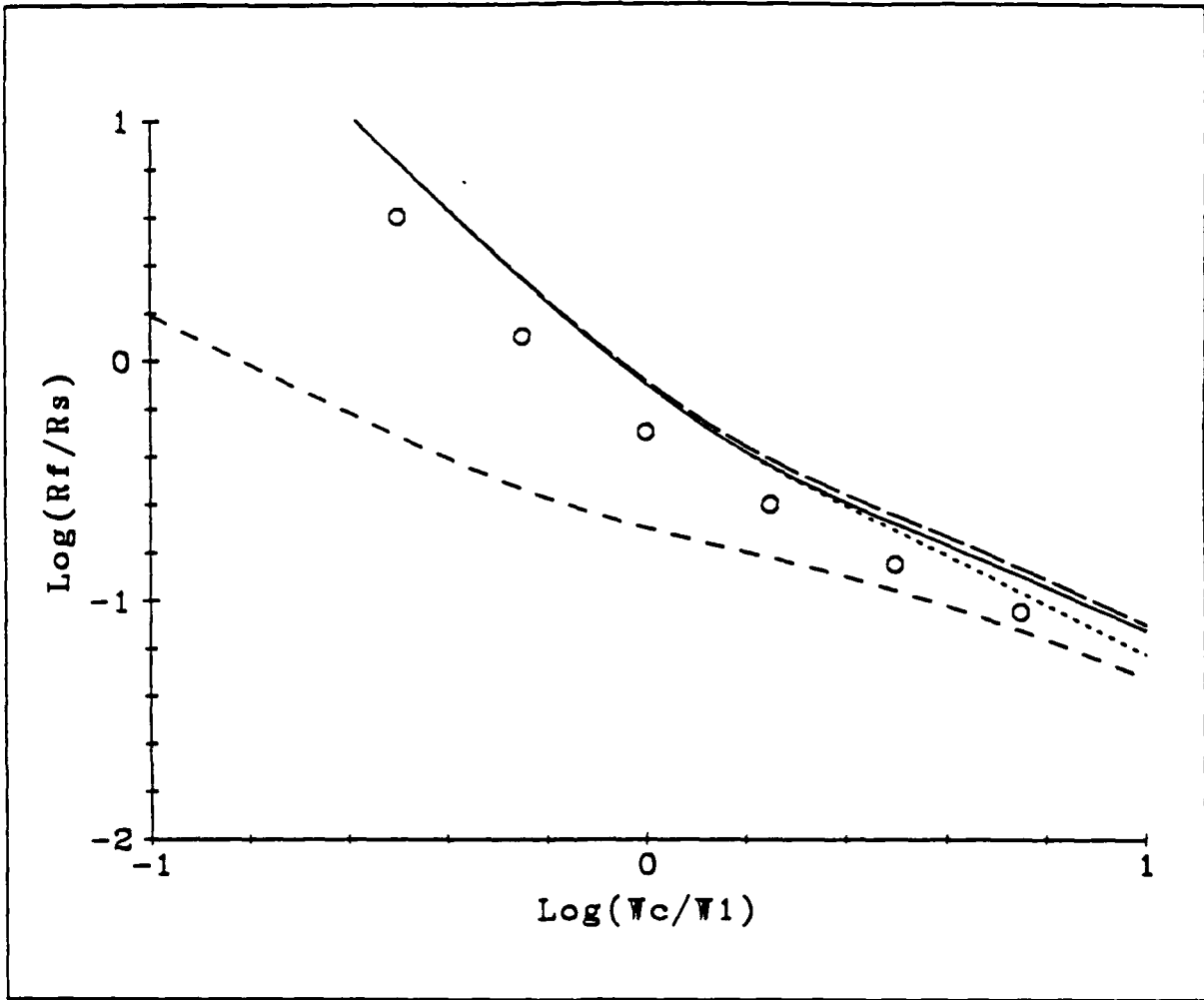


- - - - - Model I
 ————— Model II
 - · - · - · Model III
 ········· Model IV
 O O O O Simulation Data

$L/W_1 = 0.567$

$t/W_1 = 0.1$

FIGURE 8a

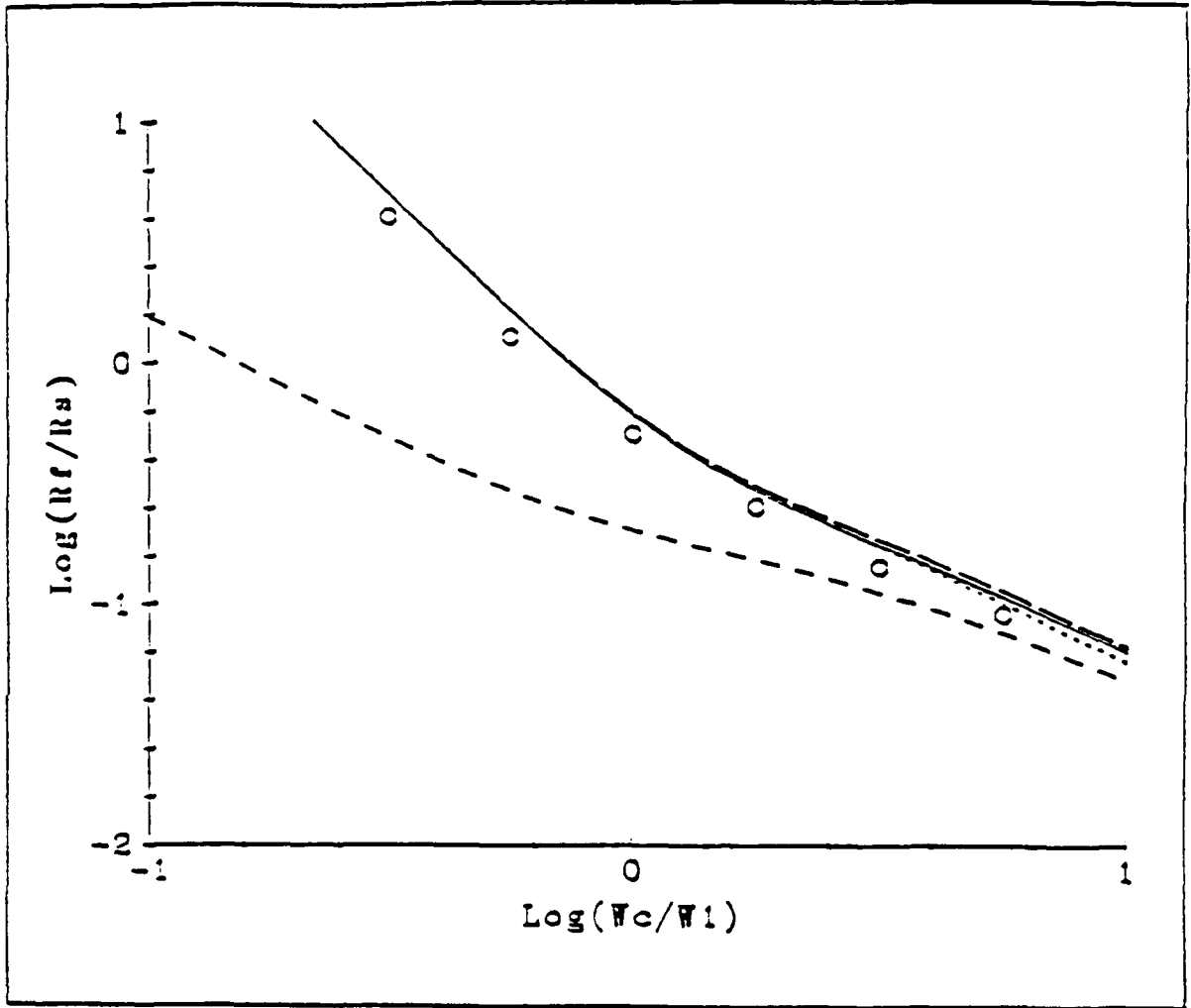


- Model I
- Model II
- · - · - Model III
- Model IV
- ○ ○ ○ Simulation Data

$L/W1=0.567$

$t/W1=0.5$

FIGURE 8b

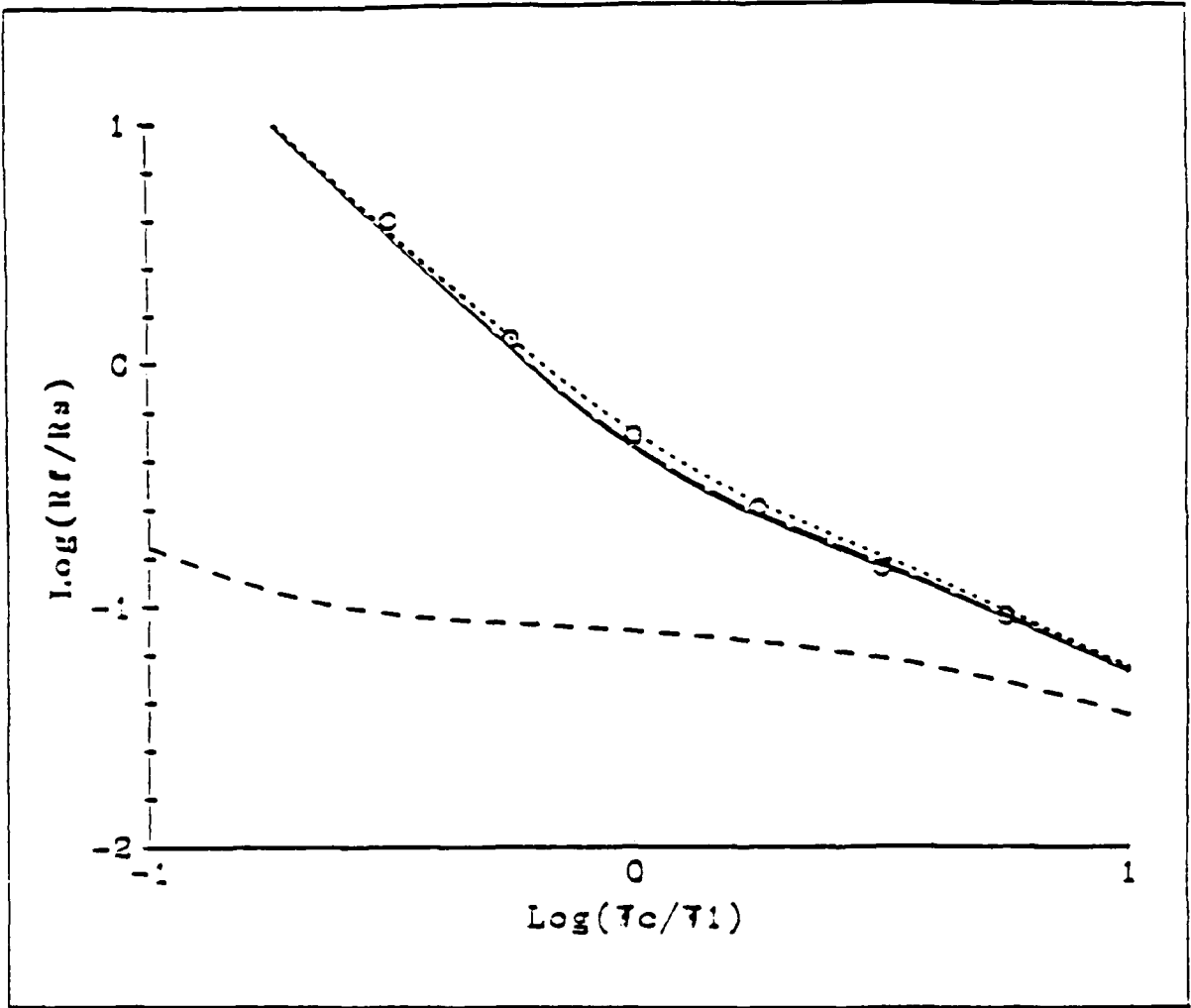


- Model I
- Model II
- · - · - Model III
- Model IV
- ○ ○ ○ Simulation Data

$L/W1=0.567$

$t/W1=1.0$

FIGURE 8c

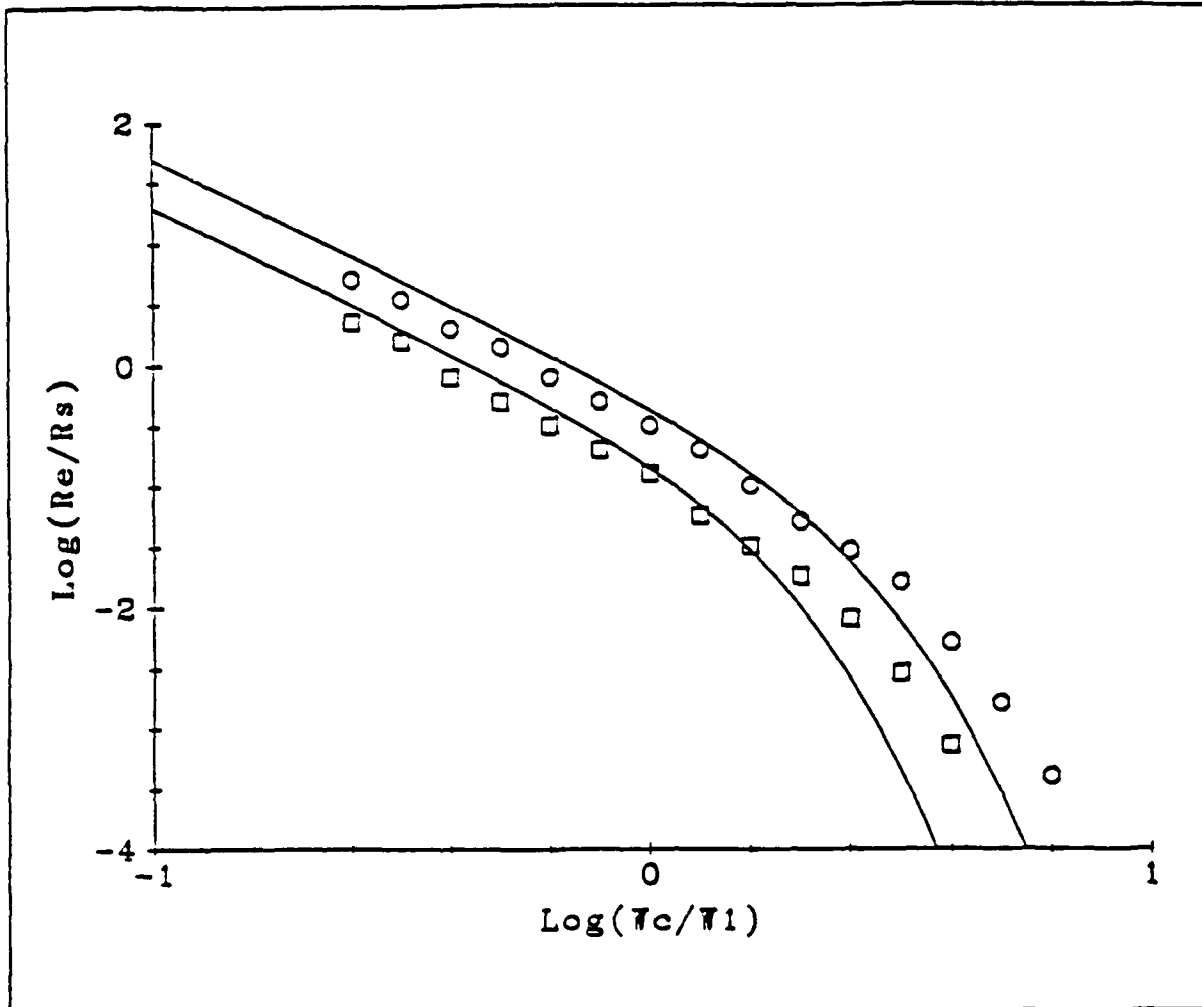


- - - - - Model I
 _____ Model II
 - · - · - Model III
 ········· Model IV
 ○ ○ ○ ○ Simulation Data

$L/W_1 = 0.567$

$t/W_1 = 10.0$

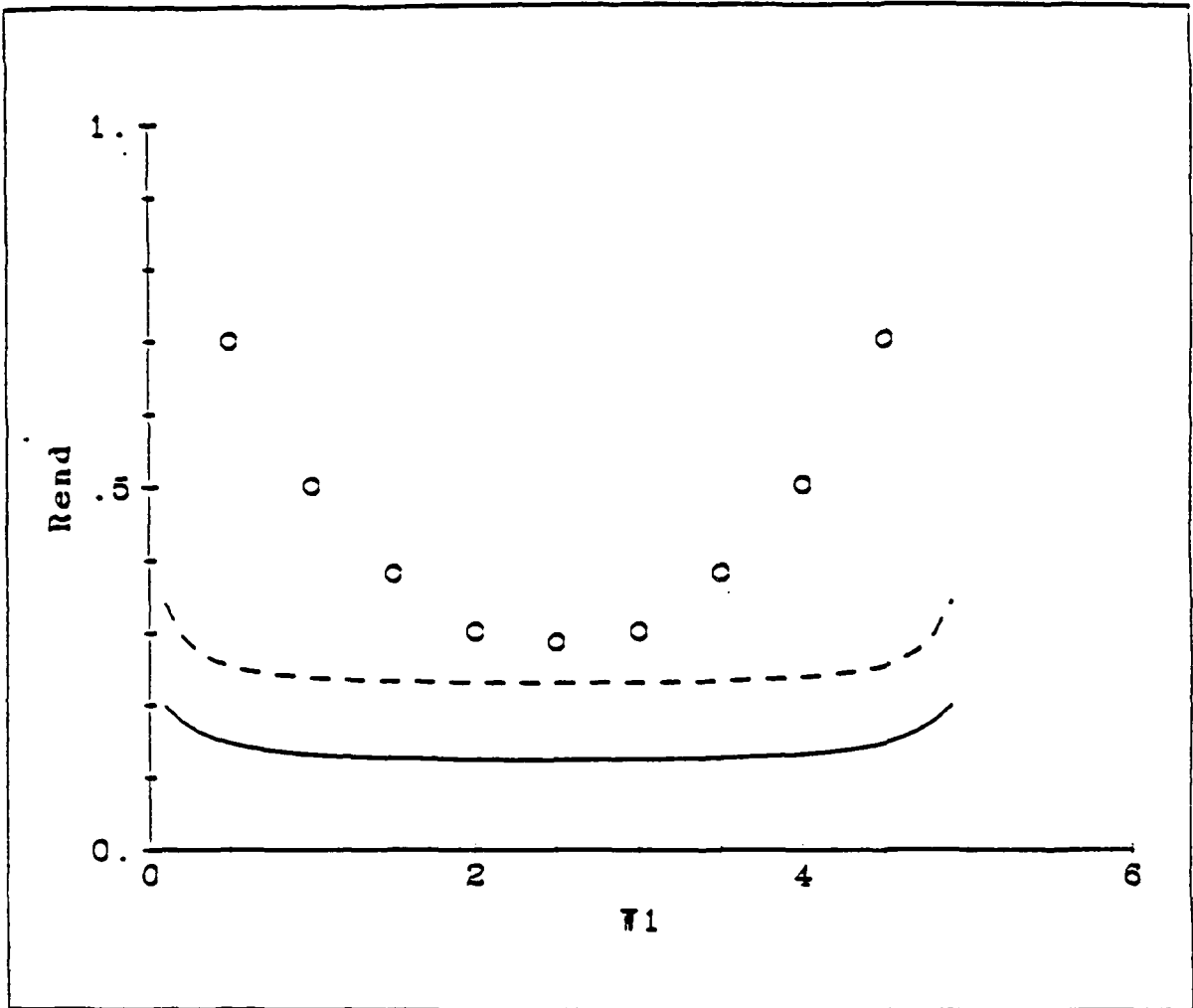
FIGURE 8d



$t/W_1=1.0$

$L/W_1=0.567, 0.358$

FIGURE 9



_____ Model II with $t=1.0$
 - - - - - Model II with $t=0.5$
 o o o o Simulation Data from [10]

FIGURE 10